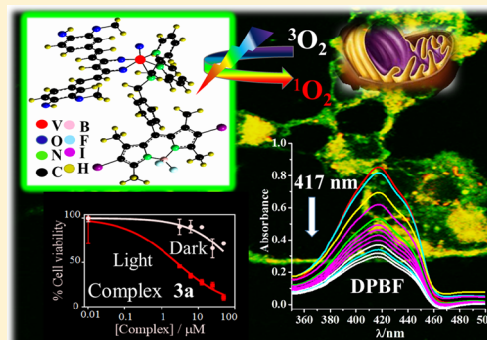


## Curcumin “Drug” Stabilized in Oxidovanadium(IV)-BODIPY Conjugates for Mitochondria-Targeted Photocytotoxicity

Utso Bhattacharyya,<sup>†</sup> Brijesh Kumar,<sup>‡</sup> Aditya Garai,<sup>†</sup> Arnab Bhattacharyya,<sup>†</sup> Arun Kumar,<sup>†</sup> Samya Banerjee,<sup>†</sup> Paturu Kondaiah,<sup>\*,‡</sup> and Akhil R. Chakravarty<sup>\*,†</sup><sup>†</sup>Department of Inorganic and Physical Chemistry and <sup>‡</sup>Department of Molecular Reproduction, Development and Genetics, Indian Institute of Science, Bangalore 560 012, India

## Supporting Information

**ABSTRACT:** Ternary oxidovanadium(IV) complexes of curcumin (Hcur), dipicolylamine (dpa) base, and its derivatives having pendant noniodinated and di-iodinated boron-dipyrromethene (BODIPY) moiety ( $L_1$  and  $L_2$ , respectively), namely,  $[\text{VO}(\text{dpa})(\text{cur})]\text{ClO}_4$  (**1**),  $[\text{VO}(L_1)(\text{cur})]\text{ClO}_4$  (**2**), and  $[\text{VO}(L_2)(\text{cur})]\text{ClO}_4$  (**3**) and their chloride salts (**1a–3a**) were prepared, characterized, and studied for anticancer activity. The chloride salts were used for biological studies due to their aqueous solubility. Complex **1** was structurally characterized by single-crystal X-ray crystallography. The complex has a  $\text{VO}^{2+}$  moiety bound to dpa ligand showing N,N,N-coordination in a facial mode, and curcumin is bound in its mono-anionic enolic form. The V–O(cur) distances are 1.950(18) and 1.977(16) Å, while the V–N bond lengths are 2.090(2), 2.130(2), and 2.290(2) Å. The bond *trans* to V=O is long due to trans effect. The complexes are stable in a solution phase over a long period of time of 48 h without showing any apparent degradation of the curcumin ligand. The diiodo-BODIPY ligand ( $L_2$ ) or Hcur alone showed limited solution stability in dark. The emissive BODIPY ( $L_1$ ) containing complex **2a** showed preferential mitochondrial localization in MCF-7 cells in cellular imaging experiments. The cytotoxicity of the complexes was studied by MTT assay. The BODIPY complex **3a** showed excellent photodynamic therapy effect in visible light (400–700 nm) giving  $\text{IC}_{50}$  values of 2–6  $\mu\text{M}$  in HeLa and MCF-7 cancer cells, while being less toxic in dark ( $\sim 100 \mu\text{M}$ ). The cell death was apoptotic in nature involving reactive oxygen species (ROS). Mechanistic data from pUC19 DNA photocleavage studies revealed photogenerated ROS as primarily  $^1\text{O}_2$  from the BODIPY moiety and  $\cdot\text{OH}$  radicals from the curcumin ligand.



## INTRODUCTION

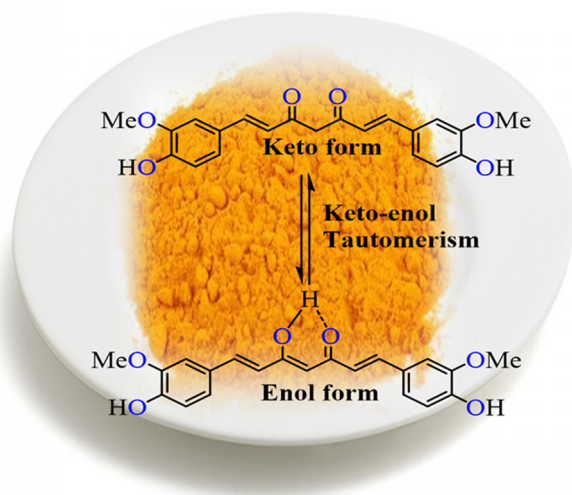
Curcumin (Hcur) as an active ingredient of turmeric is well-known for the treatment of a wide variety of ailments (Chart 1).<sup>1–10</sup> The anticancer activity is ascribed to its antiproliferative, anti-metastatic, and antiangiogenic properties. In vitro studies indicate that curcumin induces apoptosis via mitochondrial pathways comprising caspases and the Bcl-2 family of proteins and restricts the function of NF- $\kappa$ B.<sup>11–17</sup> The major predicaments are poor aqueous solubility and hydrolytic instability in buffer of physiological pH of 7.4 that limit its therapeutic potential. With a high dose of tolerance intake (>100 mg, i.e.,  $\sim 3$  g of turmeric) per day, its delivery to a biological target is restricted. Nelson and co-workers have made an elaborate analysis of the published results and highlighted the unreliability of the data leading to its classification under pan-assay interference compounds (PAINS) and invalid metabolic panaceas (IMPS).<sup>18,19</sup> A rebuttal has subsequently been made by other authors who have opined that vast literature reports on curcumin and curcuminoids cannot just be dismissed from limited observations and analysis.<sup>20</sup> The real concern of curcumin is its poor bioavailability and instability in a buffer medium. This needs to be addressed rationally and critically. Recent reports have shown that binding of curcumin

in its enolic form to an oxophilic metal ion leads to its stabilization and significantly increases its bioavailability.<sup>21–30</sup> Transition-metal complexes of curcumin show different extent of labilization of the M–O (curcumin) bond.<sup>21–24,27,28</sup> While metal ions like Co(III) and Pt(II) show slow release of curcumin from their metal complexes leading to its eventual degradation, oxophilic metal ions like vanadium(IV) or trivalent lanthanoids stabilize the ligand in a significant manner and enhance its bioavailability.<sup>21–24,27–29</sup>

The present work stems from our continued interests to design curcumin based photocytotoxic agents, and we used  $\text{VO}^{2+}$  moiety to stabilize the curcumin dye in its metal-bound form. While the stabilized curcumin is expected to retain its pendant diphenolic units (not used as metal binding site) intact for its biological activity, dipicolylamine (dpa)-based N,N,N-donor ancillary ligands with pendant di-iodinated boron-dipyrromethene (BODIPY) moiety is incorporated in the ternary structure to generate singlet oxygen ( $^1\text{O}_2$ ) for achieving light-activated cell death by a type-II pathway akin to photodynamic therapy (PDT) of cancer by hematoporphyrin

Received: July 28, 2017

Chart 1. Curcumin Dye (Hcur) and Its Structure in Keto and Enolic Forms



drug, namely, Photofrin.<sup>31–35</sup> The ligands in the ternary structure  $[(\text{BODIPY-dpa})\text{VO}(\text{cur})]^+$  are expected to show selectivity and targeted anticancer activity induced by light. The advantage of PDT over conventional chemotherapy is its selectivity causing the cellular damage of only the light-activated cancer cells, while the unexposed healthy cells remain unaffected.<sup>31,32</sup> PDT with its three essential components, specifically, (i) photosensitizer (PS), (ii) light to activate the PS, and (iii) molecular oxygen to generate reactive oxygen species (ROS), has received current attention for developing metal-based PDT agents that could overcome the toxicities associated with Photofrin, namely, skin sensitivity and hepatotoxicity.<sup>31,35</sup> The PDT agents having vanadium as a bioessential metal ion, curcumin as a nontoxic natural product (NP) for its selectivity and anticancer activity, and BODIPY units as photosensitizers could find utility as new generation metal-based PDT agents. We used two different BODIPY moieties ( $L_1$  and  $L_2$ ). The highly emissive ligand  $L_1$  is incorporated in the structure for cellular imaging to study localization of the complex in different cellular organelle, while the diiodo BODIPY unit in  $L_2$  is used as a photosensitizer to generate singlet oxygen on light activation. Additionally, curcumin as a photosensitizer is known to generate hydroxyl radicals as the ROS on light activation.<sup>1,2,7</sup>

The ternary complexes are aimed to enhance the efficacy compared to our earlier reported non-PDT oxidovanadium(IV) complexes, specifically,  $[\text{VO}(\text{cur})(\text{phen}/\text{dppz})\text{Cl}]$ , where phen and dppz are 1,10-phenanthroline and dipyrrophenazine.<sup>22</sup> These complexes showed stabilization of curcumin on binding to the  $\text{VO}^{2+}$  unit. The replacement of the phenanthroline bases by dipicolylamines with BODIPY units is to achieve enhanced PDT activity by generating singlet oxygen on photoactivation. While human body has enzymatic defense mechanism to degrade the hydroxyl radicals, a similar process is absent in our cells for the singlet oxygen. Again, the BODIPY moiety is capable of generating ROS at low oxygen concentration that is prevalent in the tumor cells. This is due to high yield of singlet oxygen from the diiodo BODIPY unit. Herein, we present the PDT activity of three ternary oxidovanadium(IV) complexes of curcumin  $[\text{VO}(\text{L})(\text{cur})]\text{X}$ , where cur is the curcumin monoanion, X is  $\text{ClO}_4$  for complexes 1–3 or Cl for complexes

1a–3a, L is dipicolylamine (dpa) for 1 and 1a, BODIPY appended dpa for 2 and 2a, and diiodo BODIPY appended dpa for 3 and 3a (Figure 1). The complexes showed aqueous

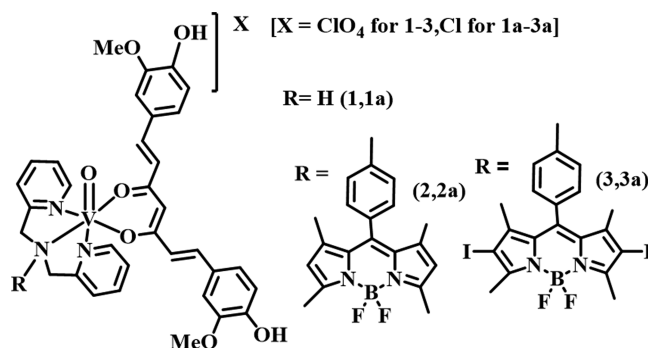


Figure 1. Ternary oxidovanadium(IV) complexes 1–3 as perchlorate and 1a–3a as chloride salts.

solubility and stability, while the ligands alone, specifically, curcumin (Hcur) and the BODIPY bases ( $L_1$  and  $L_2$ ) showed poor aqueous solubility. The significant aspects of this study include structural characterization of the curcumin complex 1 by X-ray crystallography, complex 3a having diiodo BODIPY unit showing remarkable singlet oxygen ( $^1\text{O}_2$ ) mediated photocytotoxicity in MCF-7 (human breast adenocarcinoma) and HeLa (human cervical carcinoma) cancer cells in visible light (400–700 nm), while being essentially nontoxic in dark, and the emissive complexes 1a and 2a exhibiting predominant mitochondrial localization from the confocal microscopic imaging studies. Mitochondrial localization is important, as it avoids the nuclear excision repair (NER) pathway, which reduces the efficacy of any nuclear DNA targeting anticancer drug.<sup>36,37</sup> Stabilization of curcumin in its metal-bound form could lead to further development of new strategies for cellular delivery of this dye for in vivo applications without causing any degradation or structural changes. That may enable curcumin to list out of the classification under “PAINS”.<sup>18,19</sup>

## EXPERIMENTAL SECTION

**Materials and Methods.** The reagents and chemicals were procured from the commercial sources (s.d. Fine Chemicals, India; Sigma-Aldrich, U.S.A., E-Merck and Alfa Aesar, U.K.). Solvents used were purified and distilled by standard methods.<sup>38</sup> Curcumin (95% curcuminoid content, ca. 80% curcumin) was purchased from Sigma-Aldrich, U.S.A. and purified by following a literature method.<sup>39</sup> Synthesis of the complexes was performed under nitrogen atmosphere using Schlenk technique. Supercoiled (SC) pUC19 DNA (cesium chloride purified) was from Bangalore Genie (India). Tris-(hydroxymethyl)aminomethane-HCl (Tris-HCl) buffer (pH = 7.2) was prepared using deionized and sonicated double distilled water. Dulbecco's Modified Eagle's medium (DMEM), 3-(4,5-dimethylthiazol-2-yl)-2,5-diphenyltetrazolium bromide (MTT), 2,7-dichlorofluorescein diacetate (DCFDA), calf thymus (ct) DNA, agarose (molecular biology grade), 2,2,6,6-tetramethyl-4-piperidone (TEMP), ethidium bromide (EB), Hoechst dye, propidium iodide (PI), and annexin-V/FITC were purchased from Sigma-Aldrich (U.S.A.) and used as received. The dipicolylamine (dpa), BODIPY-appended dpa ( $L_1$ ), and diiodo-BODIPY-appended dpa ( $L_2$ ) were prepared by reported procedures (4,4-difluoro-1,3,5,7-tetramethyl-4-bora-3a,4a-diaza-s-indacene is abbreviated as BODIPY in this work).<sup>40,41</sup> Tetrabutylammonium perchlorate (TBAP) was prepared by reacting tetrabutylammonium bromide and perchloric acid. **Caution!** Use in small quantities and with care.

The elemental analysis of the complexes (1–3, 1a–3a) was performed using a Thermo Finnigan FLASH EA 1112 CHNS analyzer. The infrared and electronic spectra (UV–vis) were recorded with Perkin–Elmer Lambda 35 and Perkin–Elmer spectrum one 55 spectrometers, respectively, at 25 °C. Molar conductivity measurements were made with a Control Dynamics (India) conductivity meter. Electrochemical measurements were made at 25 °C with an EG&G PAR model 253 VersaStat potentiostat/galvanostat with electrochemical analysis software 270 using a three-electrode setup having a glassy carbon working, platinum wire auxiliary, and a saturated calomel reference electrode (SCE) in dimethylformamide (DMF)–0.1 M TBAP. Electrospray ionization (ESI) mass spectral measurements were made using an Agilent Technologies 6538 UHD Accurate-mass Q-TOF LC/MS ESI model mass spectrometer. Fluorescence measurements at room temperature were done using a Perkin–Elmer LS 55 fluorescence spectrometer. The fluorescence quantum yields of the compounds were obtained by a relative method as described in the literature.<sup>22,42</sup> Viscometric measurements using ct-DNA were performed with a Schott AVS 310 automated viscometer. Fluorescence microscopic investigations were performed using ApoTome.2 fluorescence microscope. Flow cytometric analysis was performed using FACS (fluorescence-activated cell sorting) Calibur Becton Dickinson (BD) cell analyzer at FL2 channel (595 nm). Vanadium contents in 1a–3a treated MCF-7 cells were measured by Perkin–Elmer Optima 7000 DV ICP-OES.

**Synthesis of the Complexes.** Vanadyl sulfate (0.16 g, 1.0 mmol) and calcium perchlorate (0.31 g, 1.0 mmol) for 1–3 or barium chloride (0.24 g, 1.0 mmol) for 1a–3a were dissolved in 15 mL of ethanol and 3 mL of water. The mixture was then stirred at room temperature for 3 h under a nitrogen atmosphere. The mixture was filtered to remove the white calcium sulfate or barium sulfate as the precipitate. The blue filtrate was deaerated and saturated with nitrogen. To this filtrate was added a deaerated solution (10 mL of EtOH and 2 mL of MeCN) of Hcur (0.36 g, 1.0 mmol), which was previously neutralized with Et<sub>3</sub>N (0.10 g, 1.0 mmol). A deep red solution thus formed after stirring the mixture for 30 min was reacted with an ethanol solution (5 mL) of dipicolylamine (0.20 g, dpa) for 1/1a or a CH<sub>2</sub>Cl<sub>2</sub> solution (10 mL) of L<sub>1</sub> or L<sub>2</sub> (0.54 g, L<sub>1</sub>; 0.79g, L<sub>2</sub>; 1.0 mmol) for BODIPY complexes. The product precipitated out of the solution spontaneously after it was stirred for 2 h. The solid was filtered, isolated, and washed with cold ethanol, CH<sub>2</sub>Cl<sub>2</sub>, and diethyl ether and finally dried in vacuum over P<sub>4</sub>O<sub>10</sub> in a desiccator.

[VO(dpa)(cur)](ClO<sub>4</sub>) (1). Yield = 75%. Anal. Calcd for C<sub>33</sub>H<sub>32</sub>ClN<sub>3</sub>O<sub>11</sub>V: C, 54.07; H, 4.40; N, 5.73. Found: C, 53.79; H, 4.35; N, 5.44%. ESI-MS in CH<sub>3</sub>OH: *m/z* 633.1640 [M – ClO<sub>4</sub>]<sup>+</sup>. IR data/cm<sup>-1</sup>: 3360 m (br), 1590 s, 1494 vs, 1373 w, 1276 s, 1150 m, 1122 m, 1095 w, 968 m, 819 m, 619 m, 465 w (vs, very strong; s, strong; m, medium; w, weak; br, broad.). UV–visible in 1:1 dimethylformamide/Dulbecco's phosphate-buffered saline (DMF/DPBS) [ $\lambda_{\max}/\text{nm}$  ( $\epsilon/M^{-1} \text{ cm}^{-1}$ ): 715 (85), 435 (45,800), 280 (62,200)]. Molar conductivity in 10% aqueous DMF at 298 K [ $\Lambda_M/S \text{ m}^2 \text{ M}^{-1}$ ]: 97.  $\mu_{\text{eff}}$ ,  $\mu_B$  at 298 K: 1.60. [VO(dpa)(cur)]Cl (1a): Yield = 72%. Anal. Calcd for C<sub>33</sub>H<sub>32</sub>ClN<sub>3</sub>O<sub>7</sub>V: C, 59.24; H, 4.82; N, 6.28. Found: C, 58.79; H, 4.45; N, 5.95%. ESI-MS in CH<sub>3</sub>OH: *m/z* 633.1691 [M – Cl]<sup>+</sup>.

[VO(L<sub>1</sub>)(cur)](ClO<sub>4</sub>) (2). Yield = 80%. Anal. Calcd for C<sub>53</sub>H<sub>51</sub>BClF<sub>2</sub>N<sub>5</sub>O<sub>11</sub>V: C, 59.54; H, 4.81; N, 6.55. Found: C, 59.32; H, 4.47; N, 6.26%. ESI-MS in CH<sub>3</sub>OH: *m/z* 969.3458 [M – ClO<sub>4</sub>]<sup>+</sup>, IR data/cm<sup>-1</sup>: 3363 m (br), 1589 s, 1496 vs, 1368 m, 1276 s, 1154 m, 1117 m, 1094 w, 965 m, 817 m, 762 m, 619 w, 465 w, 435 m. UV–visible in 1:1 DMF/DPBS [ $\lambda_{\max}/\text{nm}$  ( $\epsilon/M^{-1} \text{ cm}^{-1}$ ): 717 (77), 501 (54 680), 454sh (36 600), 434 (35 475), 285 (61 600) (sh, shoulder)]. Molar conductivity in 10% aqueous DMF at 298 K [ $\Lambda_M/S \text{ m}^2 \text{ M}^{-1}$ ]: 89.  $\mu_{\text{eff}}$ ,  $\mu_B$  at 298 K: 1.63. [VO(L<sub>1</sub>)(cur)]Cl (2a): Yield = 78%. Anal. Calcd for C<sub>53</sub>H<sub>51</sub>BClF<sub>2</sub>N<sub>5</sub>O<sub>7</sub>V: C, 63.33; H, 5.11; N, 6.97. Found: C, 62.82; H, 4.78; N, 6.76%. ESI-MS in CH<sub>3</sub>OH: *m/z* 969.3288 [M – Cl]<sup>+</sup>.

[VO(L<sub>2</sub>)(cur)](ClO<sub>4</sub>) (3). Yield = 77%. Anal. Calcd for C<sub>53</sub>H<sub>49</sub>BClF<sub>2</sub>I<sub>2</sub>N<sub>5</sub>O<sub>11</sub>V: C, 48.19; H, 3.74; N, 5.30. Found: C, 47.93; H, 3.54; N, 4.95%. ESI-MS in CH<sub>3</sub>OH: *m/z* 1221.1298 [M – ClO<sub>4</sub>]<sup>+</sup>,

IR data/cm<sup>-1</sup>: 3364 m (br), 1588 s, 1495 vs, 1421 m, 1365 w, 1271 s, 1152 m, 1116 m, 1095 m, 969 m, 843 w, 756 m, 525 w, 465 w. UV–visible in 1:1 DMF/DPBS [ $\lambda_{\max}/\text{nm}$  ( $\epsilon/M^{-1} \text{ cm}^{-1}$ ): 721 (69), 535 (30 285) 432 (27 450), 288 (65 000)]. Molar conductivity in 10% aqueous DMF at 298 K [ $\Lambda_M/S \text{ m}^2 \text{ M}^{-1}$ ]: 84.  $\mu_{\text{eff}}$ ,  $\mu_B$  at 298 K: 1.61. [VO(L<sub>2</sub>)(cur)]Cl (3a): Yield = 75%. Anal. Calcd for C<sub>53</sub>H<sub>49</sub>BClF<sub>2</sub>I<sub>2</sub>N<sub>5</sub>O<sub>7</sub>V: C, 50.64; H, 3.93; N, 5.73. Found: C, 50.43; H, 3.74; N, 5.53%. ESI-MS in CH<sub>3</sub>OH: *m/z* 1221.0482 [M – Cl]<sup>+</sup>.

**Solubility.** The perchlorate and chloride complexes were soluble in ethanol, methanol, acetonitrile, DMF, and dimethyl sulfoxide (DMSO). The complexes were moderately soluble in CHCl<sub>3</sub> and CH<sub>2</sub>Cl<sub>2</sub> and insoluble in hydrocarbon solvents. The chloride complexes showed better aqueous solubility (~200  $\mu\text{M}$  in 99:1 v/v DPBS/DMSO) than that of perchlorate complexes (~100  $\mu\text{M}$  in 99:1 v/v DPBS/DMSO) and were used for biological studies.

**X-ray Crystallographic Procedures.** The crystal structure of [VO(dpa)(cur)]ClO<sub>4</sub> (1) was obtained by single-crystal X-ray diffraction method.<sup>43–45</sup> Single crystals were obtained upon vapor diffusion of diethyl ether into solution of the complex in acetonitrile. A crystal of dimensions 0.6 × 0.3 × 0.2 mm<sup>3</sup> was mounted on a crystal mounting loop with the help of paratone oil. The intensity data were collected using graphite-monochromated Mo K $\alpha$  radiation (0.7107 Å) at 273 K. The data quality was found to be poor. That resulted in some high thermal parameters, higher shift/esd residue for the final cycle of refinement, and relatively high *R*-indices than desired. The structure was solved in P1 space group, although there were two similar complex molecules in the unit cell. Our attempts to use centrosymmetric P $\bar{1}$  space group with *Z* value of 2 did not yield the structure. On careful analysis it was found that two molecules are not identical. While one cationic complex was involved in H-bonding with a ClO<sub>4</sub><sup>-</sup> anion, the other was not. This was supported from the Fourier transform infrared (FT-IR) data that showed splitting of the perchlorate peak indicating lowering of symmetry from *T<sub>d</sub>* to *C<sub>3v</sub>* on H-bond formation. The structure solved by direct methods using SHELXL-2014 incorporated in WinGX (Version 1.63.04a) did not show any anomaly in the core structure of the complex. Selected crystallographic parameters are given in Table 1. The CCDC deposition number is 1543636.

**Table 1. Selected Crystallographic Data for the Complex [VO(dpa)(cur)](ClO<sub>4</sub>) (1)**

empirical formula	C <sub>33</sub> H <sub>32</sub> ClN <sub>3</sub> O <sub>11</sub> V
formula weight (g M <sup>-1</sup> )	733.02
crystal system	triclinic
space group	P1
<i>a</i> , Å	12.241(3)
<i>b</i> , Å	12.600(3)
<i>c</i> , Å	12.941(3)
$\alpha$ , deg	95.769(6)
$\beta$ , deg	110.364(5)
$\gamma$ , deg	114.313(5)
<i>V</i> , Å <sup>3</sup>	1634.2(7)
<i>Z</i>	2
<i>T</i> , K	273 (2)
$\rho_{\text{calc}}$ g cm <sup>-3</sup>	1.484
$\lambda$ , Å (Mo K $\alpha$ )	0.710 73
$\mu$ , cm <sup>-1</sup>	0.452
data/restraints/parameters	14 768/15/733
F(000)	753
GOF	0.931
$R(F_o)$ , <sup>a</sup> $I > 2\sigma(I)$ [ $R_w(F_o)$ ] <sup>b</sup>	0.1102 [0.4032]
$R$ [ $R_w$ (all data)]	0.1513 [0.2289]
largest diff peak and hole (e Å <sup>-3</sup> )	0.407, -0.322

$$^a R = \sum ||F_o| - |F_c|| / \sum |F_o|. \quad ^b R_w = \{ \sum [w(F_o^2 - F_c^2)^2] / \sum [w(F_o^2)] \}^{1/2}. \\ w = [ \sigma^2 F_o^2 + (0.0723P)^2 ]^{-1}, \text{ where } P = (F_o^2 + 2F_c^2) / 3.$$

Table 2. Selected Physicochemical Data for the Complexes 1–3 as Perchlorate Salts

complex	IR, <sup>a</sup> cm <sup>-1</sup> V=O, C=O	$\lambda_{\text{max}}$ , nm ( $\epsilon^b$ , M <sup>-1</sup> cm <sup>-1</sup> )	$\lambda_{\text{F}}$ , <sup>c</sup> nm [ $\Phi_{\text{F}}$ ]	$\mu_{\text{eff}}^d$	$\Lambda_{\text{M}}^e$	$E_{\text{pc}}^f$ V	$K_{\text{b}}^g$ M <sup>-1</sup>
1	968, 1590	435(45,800), 715(85)	531 [0.04]	1.60	97	-1.02	$(8.9 \pm 0.4) \times 10^4$
2	965, 1589	434(35,475), 501(54,680), 717(77)	512 [0.11]	1.63	89	-0.96	$(2.1 \pm 0.6) \times 10^5$
3	969, 1588	432(27,450), 535(30,285), 721(69)	521 [0.01]	1.61	84	-1.04	$(7.9 \pm 0.5) \times 10^4$

<sup>a</sup>In the solid phase. <sup>b</sup>In 1:1 DMF–DPBS buffer. <sup>c</sup>In 10% aqueous DMSO. Quantum yield was measured using fluorescein as the standard ( $\Phi_{\text{F}} = 0.79$ ). <sup>d</sup> $\mu_{\text{eff}}$  in  $\mu_{\text{B}}$  for solid samples of the complexes at 25 °C. <sup>e</sup> $\Lambda_{\text{M}}$ , molar conductivity ( $\text{S m}^2 \text{M}^{-1}$ ) in 10% aqueous DMF at 25 °C. <sup>f</sup>In 5 mL of DMF with 0.1 M TBAP and 2 mmol complexes. The potentials were vs SCE at a scan rate of 50 mV s<sup>-1</sup>.  $E_{\text{pc}}$  is the cathodic peak potential. There was no anodic counterpart. <sup>g</sup>Intrinsic ct-DNA binding constant.

**Theoretical Methods.** The geometries of the complexes were optimized by density functional theory (DFT) using B3LYP level of theory and LanL2DZ basis state by Gaussian 09 program.<sup>46–48</sup> The coordinates were initially obtained from the crystal structure of complex 1. They were used for optimization of the structures of the complexes with or without having the BODIPY moiety. The optimized coordinates are given in Tables S1–S3 along with the electronic transitions in Figure S17 (see Supporting Information).

**Experiments on Singlet Oxygen.** Generation of singlet oxygen on visible light irradiation of the complexes was examined using 1,3-diphenylisobenzofuran (DPBF) titration method.<sup>49,50</sup> DPBF and the complex in DMSO in a 50:1 molar ratio were taken and photo-irradiated. The absorption maximum at 417 nm corresponding to DPBF was monitored after different time intervals of the light exposure using a broad-band light source of 400–700 nm (Luzchem Photoreactor model LZC-1, Ontario, Canada, fitted with Sylvania-made 8 fluorescent white tubes, having a fluorescence rate of 2.4 mW cm<sup>-2</sup>, to provide a total dose of 10 J cm<sup>-2</sup>). The relative rates of decay of the DPBF-based absorption band for different complexes and the BODIPY ligands were calculated.

**Cellular Measurements.** Cytotoxicity studies were performed with the complexes 1a–3a in MCF-7 (human breast adenocarcinoma cell line) and HeLa (human epithelial cervical carcinoma cell line) by 3-(4,5-dimethylthiazol-2-yl)-2,5-diphenyl tetrazolium bromide (MTT) colorimetric assay following procedures that were reported earlier.<sup>51</sup> Cells were incubated with various concentrations of 1a–3a for 4 h in dark. One set of cells was exposed to visible light (400–700 nm Luzchem Photoreactor, 10 J cm<sup>-2</sup> power) for 1 h, while the other set was kept in darkness. The stability of the cells with this light dose was ascertained prior to the exposure of the samples containing the complexes. Data were obtained with use of three independent sets of experiments performed in triplicates for each concentration. Uptake of the complexes in MCF-7 cells was studied by flow cytometry. 2',7'-Dichlorofluorescein diacetate (DCFDA) assay was performed with the complexes to detect generation of any ROS in the MCF-7 cells. The final concentration of vanadium content in 1a–3a-treated MCF-7 cells were measured by inductively coupled plasma mass spectrometry (ICP-MS) method. The cellular localization of fluorescent complexes 1a and 2a inside the MCF-7 cells was performed by confocal microscopy experiments. Different organelle selective trackers were used for cellular localization study using the merged images. The effect of the complexes on cell cycle in MCF-7 was studied to analyze the phase where the cell cycle got arrested, and annexin-V/FITC assay was performed to confirm apoptotic cell death.

**DNA Binding and Cleavage Experiments.** UV–vis spectral studies were done to determine DNA binding constants of the complexes using calf thymus (ct) DNA by reported procedures.<sup>52</sup> Viscosity measurements were performed to ascertain the DNA binding nature of the complexes 1a–3a compared to ethidium bromide (EB) as a DNA intercalator and Hoechst dye as a DNA groove binder. The supercoiled (SC) pUC19 plasmid DNA photocleavage activity of the complexes was studied on light exposure using diode lasers followed by gel electrophoresis. A monochromatic visible light source of 532 nm (100 mW power, 1 h exposure time, 0.32 ± 0.02 mm beam

diameter) was used from a continuous-wave (CW) diode laser made of Research Electro-Optics, Colorado (U.S.A.), model no. EXLSR-532–100-CDRH. Different external agents, namely, sodium azide and 2,2,6,6-tetramethyl-4-piperidone (TEMP) as singlet oxygen quenchers, DMSO, KI, and catalase as hydroxyl radical scavengers, and superoxide dismutase (SOD) for superoxide scavenger were used for mechanistic studies to ascertain the formation of any hydroxyl radicals ( $\cdot\text{OH}$ ) and singlet oxygen ( $^1\text{O}_2$ ) as the ROS. D<sub>2</sub>O was used as a solvent in which singlet oxygen is known to have longer lifetime than in H<sub>2</sub>O.<sup>53</sup>

## RESULTS AND DISCUSSION

**Synthesis and General Aspects.** Ternary oxidovanadium(IV) complexes of curcumin (Hcur) having dipicolylamine (dpa) bases, namely, [VO(dpa)(cur)]X (X = ClO<sub>4</sub><sup>-</sup>, 1; Cl, 1a), [VO(L<sub>1</sub>)(cur)]X (L<sub>1</sub> = BOPIPY-appended dpa; X = ClO<sub>4</sub><sup>-</sup>, 2; Cl, 2a) and [VO(L<sub>2</sub>)(cur)]X (L<sub>2</sub> = diiodo BOPIPY-appended dpa; X = ClO<sub>4</sub><sup>-</sup>, 3; Cl, 3a), were prepared in good yield from a general synthetic procedure in which vanadyl sulfate was first reacted with calcium perchlorate or barium chloride, respectively, for the perchlorate or chloride counteranion, in aqueous ethanol (1:5 v/v), and the filtrate on removal of calcium sulfate or barium sulfate was subsequently reacted with the deprotonated solution of curcumin in ethanol–acetonitrile mixture. Finally, a solution of the tridentate ligand (in ethanol for dpa or in CH<sub>2</sub>Cl<sub>2</sub> for L<sub>1</sub> and L<sub>2</sub>) was added to the reaction mixture to obtain a precipitate of the desired product. The complexes were characterized from spectroscopic and analytical data. Selected physicochemical data are given in Table 2. The electrospray ionization mass spectrometry (ESI-MS) data of the perchlorate and chloride complexes showed respective single peak of [M – ClO<sub>4</sub>]<sup>+</sup> or [M – Cl]<sup>+</sup> in MeOH (Figures S1–S6, Supporting Information). The complexes were 1:1 electrolytes in 10% aqueous DMF giving molar conductivity values of ca. 90 S m<sup>2</sup> M<sup>-1</sup> at 25 °C.<sup>54</sup> The magnetic moment values of ~1.6  $\mu_{\text{B}}$  indicate V(IV) oxidation state with one unpaired electron. The IR spectra of the complexes showed C=O and C=C stretching bands assignable to curcumin at ~1589 and ~1495 cm<sup>-1</sup>, respectively (Figures S7–S9, Supporting Information). The characteristic infrared bands of V=O and ClO<sub>4</sub><sup>-</sup> anion were observed at ca. 967 and 1095 cm<sup>-1</sup>, respectively.<sup>55</sup> The ClO<sub>4</sub><sup>-</sup> peak showed splitting suggesting deviation from its T<sub>d</sub> geometry to a lower symmetry, possibly due to hydrogen-bonding interaction with the complex in the solid state (Figure S10, Supporting Information). The oxidovanadium(IV) complexes showed a broad and weak d–d band within 715–720 nm in 1:1 DMF/DPBS medium (Figure S11, Supporting Information).<sup>21,49,56</sup> An intense visible band at ~434 nm with a shoulder at ~454 nm is assigned to curcumin  $\pi \rightarrow \pi^*$  transition with the shoulder peak being prominent in complex 2

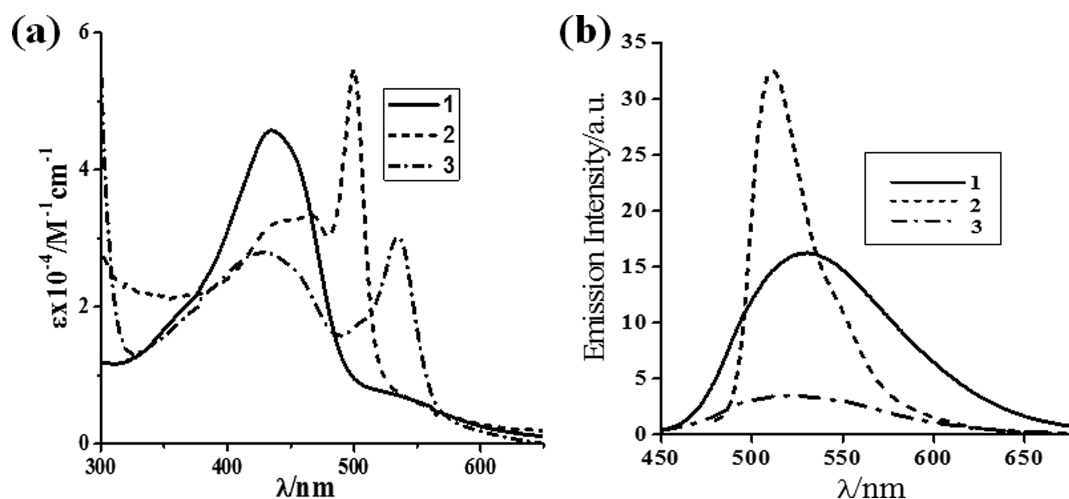


**Figure 2.** (a) Absorption spectra of the complexes 1–3 in 1:1 (v/v) DMF/PBS buffer medium. (b) Emission spectra of the complexes 1–3 in 10% aqueous DMSO ( $\lambda_{\text{exc}}$ : 430 nm for 1 and 3; 465 nm for 2).

(Figure 2a).<sup>7</sup> The BODIPY and diiodo BODIPY-centered intense  $\pi \rightarrow \pi^*$  transition was observed for complexes 2 and 3 at 501 and 535 nm, respectively.<sup>39,40</sup> This band was not visible in the spectrum of complex 1, which lacks a BODIPY moiety. The dpa ligand showed an intense band in the complexes at  $\sim 280$  nm. All the complexes were found to be emissive in 10% aqueous DMSO (Figure 2b). Complexes 1 and 3 showed respective emission maxima at 531 and 521 nm upon excitation at 430 nm. The emission of complex 1 in absence of the BODIPY moiety is due to curcumin giving a  $\phi_F$  value of 0.04. The emission of complex 3 with a  $\phi_F$  value of 0.01 is also due to curcumin as the diiodo BODIPY moiety being nonemissive due to efficient intersystem crossing (ISC).<sup>57–59</sup> Complex 2 is highly emissive due to combined green emission of curcumin and the BODIPY unit in  $L_1$  giving a band at 512 nm with a modest  $\phi_F$  value of 0.11 upon excitation at 465 nm. The emission spectral property of 2 makes it suitable for cellular uptake and imaging studies by confocal fluorescence microscopy. The complexes were redox-active showing a reduction peak assignable to the V(IV)–V(III) couple near  $-1.0$  V versus SCE in DMF with 0.1 M  $[\text{Bu}_4\text{N}](\text{ClO}_4)$  (TBAP) as the supporting electrolyte (Table 2, Figure S12, Supporting Information). The curcumin-based reduction peaks in 1–3 were observed near  $-1.59$  V. Complex 2 showed a BODIPY-based reduction peak near  $-1.17$  V. The complexes did not show any oxidative response. The redox stability of the complexes over a large potential window is expected to decrease their chemical nuclease activity and dark cellular toxicity in the presence of thiols, namely, glutathione (GSH). The redox stability of the metal is also expected to reduce the possibility of any curcumin ligand release.

**Stability of the Complexes.** Limited stability of curcumin in the physiological buffer medium makes it unsuitable for varied medicinal applications.<sup>7,18,19</sup> Curcumin is known to degrade via different pathways, namely, (i) reduction, (ii) conjugation, (iii) oxidation, and (iv) cleavage to form vanillin, ferulic acid, and feruloylmethane as the major products. One reason for the classification of curcumin under “PAINS” and “IMPS” is due to its instability. Our earlier reports have shown that binding of curcumin to a metal ion leads to its stability.<sup>21,22</sup> Cobalt(III) and platinum(II) complexes slowly release curcumin on chemical and/or photochemical treatments.<sup>23,24,27</sup>

In contrast, oxophilic metal ions do not show any release of

curcumin as evidenced from the absorption spectral studies of the complexes.<sup>21,22,29</sup> The present complexes were found to be stable in both solid and solution phases under dark experimental conditions. The spectral band intensity of curcumin alone or in its metal-bound state was monitored by absorption spectroscopy in 1:1 DMF/DPBS medium up to 48 h. The intensity of the spectral band remained essentially unchanged compared to that of free curcumin (Figure 3, Figure

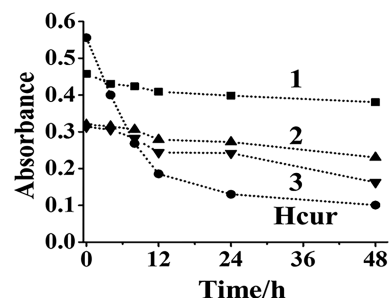


**Figure 3.** Absorption spectral traces of the complexes 1–3 and curcumin (Hcur) (monitored at 435 nm for 1, 2 and curcumin; 432 nm for 3) in 1:1 (v/v) DMF/PBS buffer medium (pH = 7.2) at 37 °C up to 48 h indicating the stability of the  $\text{VO}^{2+}$  bound curcumin.

S13, Supporting Information). The stability follows the order: 1 > 2 > 3. The spectra of BODIPY complex 2 remained unchanged up to 48 h, while the diiodo-BODIPY complex 3 showed reduced band intensity, possibly due to instability of the ligand.<sup>60,61</sup> A similar trend was observed for the chloride analogues (1a–3a) when their stabilities were spectroscopically monitored in DMSO–DMEM medium (1:99 v/v, similar to cellular medium) for 72 h (Figure S14, Supporting Information). The spectral data revealed curcumin stability on binding to  $\text{VO}^{2+}$  in buffer at pH of 7.2. Furthermore, ESI-MS spectral studies showed that complex 2 even after 1 h of photo-irradiation (400–700 nm) displayed  $\sim 65\%$  of the complex remaining intact giving a peak of  $[\text{M}-\text{ClO}_4]^+$  in MeOH with an  $m/z$  value of 969.3287 (Figure S15, Supporting Information).

**X-ray Crystal Structure.** The crystal structure of  $[\text{VO}(\text{dpa})(\text{cur})]\text{ClO}_4$  (1) was obtained by single-crystal X-ray diffraction method. A perspective view of the cationic complex

in **1** is shown in Figure 4 (Figure S16, Supporting Information). Selected bond distances and angles are given in Table 3. The

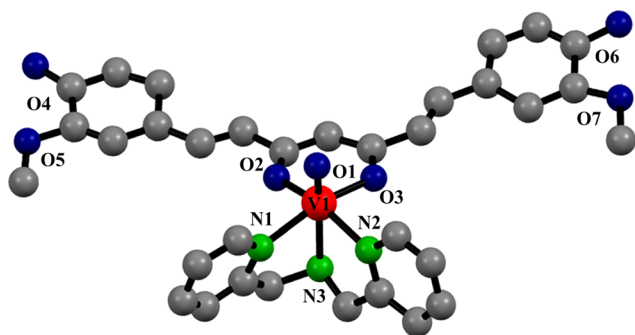


**Figure 4.** A perspective view of the cationic complex in  $[\text{VO}(\text{dpa})(\text{cur})](\text{ClO}_4)$  (**1**) showing the spatial arrangements of the ligands in the ternary structure (color code: red, V; green, N; blue, O; gray, C). The hydrogen atoms are omitted for clarity.

**Table 3.** Selected Bond Distances (Å) and Angles (deg) for  $[\text{VO}(\text{dpa})(\text{cur})](\text{ClO}_4)$  (**1**)

V(1)–O(1)	1.559(16)	O(3)–V(1)–N(1)	162.40(9)
V(1)–O(2)	1.950(18)	O(1)–V(1)–N(2)	93.20(9)
V(1)–O(3)	1.977(16)	O(2)–V(1)–N(2)	157.80(8)
V(1)–N(1)	2.090(2)	O(3)–V(1)–N(2)	85.6(7)
V(1)–N(2)	2.130(2)	O(1)–V(1)–N(3)	163.70(9)
V(1)–N(3)	2.290(2)	O(2)–V(1)–N(3)	87.00(8)
O(1)–V(1)–O(2)	104.40(9)	O(3)–V(1)–N(3)	83.70(8)
O(1)–V(1)–O(3)	107.20(8)	N(1)–V(1)–N(2)	92.80(8)
O(2)–V(1)–O(3)	88.00(7)	N(2)–V(1)–N(3)	74.50(8)
O(1)–V(1)–N(1)	93.20(9)	N(1)–V(1)–N(3)	75.96(8)
O(2)–V(1)–N(1)	85.60(9)		

unit-cell packing diagram showed the presence of two similar cationic complexes and two lattice perchlorate anions (Figure S17, Supporting Information). One perchlorate is hydrogen-bonded to the complex involving the dpa ligand, while the other perchlorate does not show any such interaction. The X-ray structural observation is buttressed from the FT-IR data showing splitting of the IR band of the perchlorate group (Figure S10, Supporting Information). This interaction, however, has no impact on the core structure of the curcumin ligand bound to the oxidovanadium(IV) moiety. The ternary structure of the complex has a distorted octahedral  $\text{VO}_3\text{N}_3$  core in which the tridentate N,N,N-donor dipicolylamine (dpa) base is bonded to the oxidovanadium(IV) unit in a facial mode, and the monoanionic curcumin (cur) ligand in its enolic form is bonded in a O,O-bidentate chelating mode thus making the complex as monocationic with the perchlorate as the counteranion. The V–O(cur) distances are of 1.950(18) and 1.977(16) Å. The V–N bond lengths are 2.090(2), 2.130(2), and 2.290(2) Å. The V=O bond is of 1.559(16) Å. The bond *trans* to the V=O bond is the longest among V–N (2.290(2) Å) due to trans effect. The N–H group of dpa is hydrogen-bonded to  $\text{ClO}_4$  giving a distance of 2.053(2) Å. The M–O(cur) bond distances in the structurally characterized curcumin complexes are within 1.878(4) to 2.410(4) Å, where M is a transition metal or lanthanoid (Table S4, Supporting Information).<sup>21–23,25,26,29</sup> The Co(III) curcumin complex exhibits a M–O(cur) bond length of  $\sim 1.88$  Å. This complex releases curcumin only upon chemical reduction by

glutathione or on photoactivation to form Co(II) species.<sup>23,24</sup> The redox stable VO(IV), La(III), and Gd(III) complexes with respective M–O(cur) distances of  $\sim 1.95$ ,  $\sim 2.40$ , and  $\sim 2.41$  Å do not show similar release of curcumin.<sup>21,22,29,30</sup>

**Theoretical Studies.** DFT studies were done to rationalize the structural and spectral data of complexes **1–3** using B3LYP with Lanl2DZ basis set with Gaussian programs.<sup>45–47</sup> The coordinates obtained from the crystal structure of complex **1** were used for the geometrical optimization of the complexes (Tables S1–S3, Supporting Information). The optimized structures along with the highest occupied molecular orbital–lowest unoccupied molecular orbital (HOMO–LUMO) are shown in Figure 5. From the frontier molecular orbital (FMO)

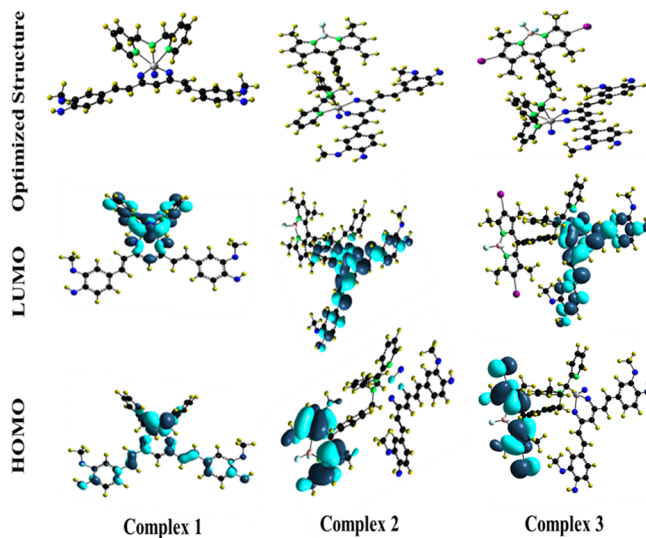


**Figure 5.** Optimized Structures and FMOs of the complexes **1–3**.

pictures it is evident that the HOMO for complex **1** is located over the curcumin moiety with significant contribution of metal and dipicolyl amine ligand, while the LUMO contains both metal and dipicolyl amine moiety. The HOMO for complexes **2** and **3** is found to be exclusively located over the BODIPY and diiodo-BODIPY core, respectively, whereas LUMO is predominantly located over curcumin and metal for both the complexes. The M–O(cur) distances are found to be  $\sim 1.92$ ,  $\sim 2.03$ , and  $\sim 2.04$  Å for **1–3**, respectively. Energy difference between LUMO and HOMO for the complexes is  $\sim 2.30$  eV (Figure S18, Supporting Information).

**Cytotoxicity.** Complexes **1a–3a** showed significant cellular uptake in MCF-7 breast cancer cells within 2 h, and the uptake was  $\sim 90\%$  within 4 h (Figure S19, Supporting Information). The vanadium metal content inside the MCF-7 cells was measured for complexes **1a–3a** by ICP-MS after 4 h of incubation and found to be 125, 150, and 133 ng/ $1 \times 10^5$  cells, respectively. The efficacy of the complexes as anticancer agents was tested using MCF-7 and cervical HeLa cancer cells in the dark and upon photo-irradiation with a broad-band visible light source (400–700 nm; Luzchem photoreactor, 10 J  $\text{cm}^{-2}$ ; irradiation time of 1 h) by MTT assay. The complexes were incubated for 4 h and then irradiated with the visible light. Dark controls were utilized to estimate the effect of light activation. Cytotoxicity was measured from the  $\text{IC}_{50}$  values (50% inhibitory concentration) obtained from the cell viability assay. The data are given in Table 4, and the  $\text{IC}_{50}$  values are compared with related complexes.<sup>22,41,62–65</sup> A bar diagram

Table 4. IC<sub>50</sub> (μM) Values of the Complexes 1a–3a as Chloride Salts and Relevant Compounds

compound	MCF-7		HeLa		ROS type <sup>c</sup>
	IC <sub>50</sub> (μM) dark <sup>a</sup>	IC <sub>50</sub> (μM) light <sup>b</sup>	IC <sub>50</sub> (μM) dark <sup>a</sup>	IC <sub>50</sub> (μM) light <sup>b</sup>	
1a <sup>d</sup>	94 ± 2	8.8 ± 0.4	>100	15.5 ± 0.9	·OH
2a <sup>d</sup>	87 ± 2	6.2 ± 0.2	>100	5.8 ± 0.5	<sup>1</sup> O <sub>2</sub> , ·OH
3a <sup>d</sup>	99 ± 3	2.7 ± 0.4	55 ± 2	2.5 ± 0.2	<sup>1</sup> O <sub>2</sub> , ·OH
curcumin (Hcur) <sup>e</sup>	90 ± 5	20 ± 2	85 ± 4	8.2 ± 0.2	·OH
[VO(cur)(dppz)Cl] <sup>f</sup>			>50	3.3 ± 0.4	·OH
[VO(L <sub>2</sub> )Cl <sub>2</sub> ] <sup>g</sup>	>50	3.4 ± 0.4	>50	1.8 ± 0.6	<sup>1</sup> O <sub>2</sub>
[Cu(L <sub>1</sub> )(cur)Cl] <sup>h</sup>			29.1 ± 0.5	7.9 ± 0.3	
[Cu(L <sub>2</sub> )(cur)Cl] <sup>h</sup>			32.1 ± 0.4	3.8 ± 0.2	
Photofrin <sup>i</sup>		2.0 ± 0.2	>41	4.3 ± 0.2	<sup>1</sup> O <sub>2</sub>
Cisplatin <sup>j</sup>	2.0 ± 0.3		24		

<sup>a</sup>The sample on incubation for 4 h in the dark. MTT assay was done using maximum complex concentration of ~100 μM. <sup>b</sup>The sample on photoexposure for 1 h in visible light of 400–700 nm at 10 J cm<sup>-2</sup>. <sup>c</sup>ROS is reactive oxygen species. <sup>d</sup>The solvent medium 99:1 (v/v) DMEM medium/DMSO. <sup>e</sup>Curcumin alone under similar experimental conditions as used for the complexes 1a–3a (ref 22). <sup>f</sup>dppz is dipyrrophenazine. The data are from ref 22. <sup>g</sup>The data from ref 48. <sup>h</sup>The data are from ref 41. Light used was 400–700 nm (power: 10 J cm<sup>-2</sup>). The nature of ROS was not reported. <sup>i</sup>The data are from refs 62 and 63 (light source: 633 nm at 5 J cm<sup>-2</sup> for 2 h). <sup>j</sup>The data are from refs 64 and 65 (IC<sub>50</sub> values for HeLa on 4 h of incubation, whereas it is 96 h of incubation for MCF-7).

giving the IC<sub>50</sub> values is shown in Figure 6 (Figures S20–S22, Supporting Information). The complexes showed remarkable

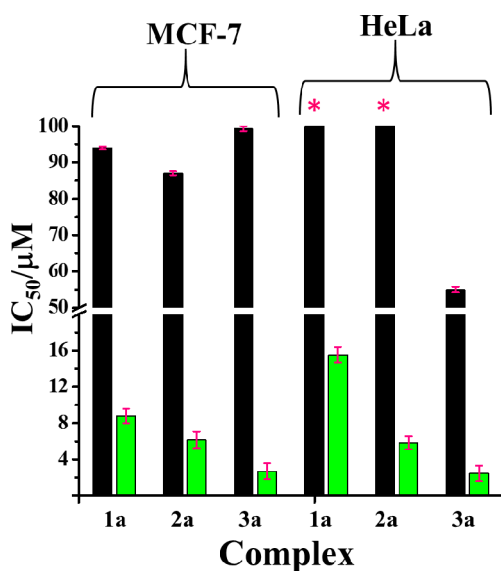


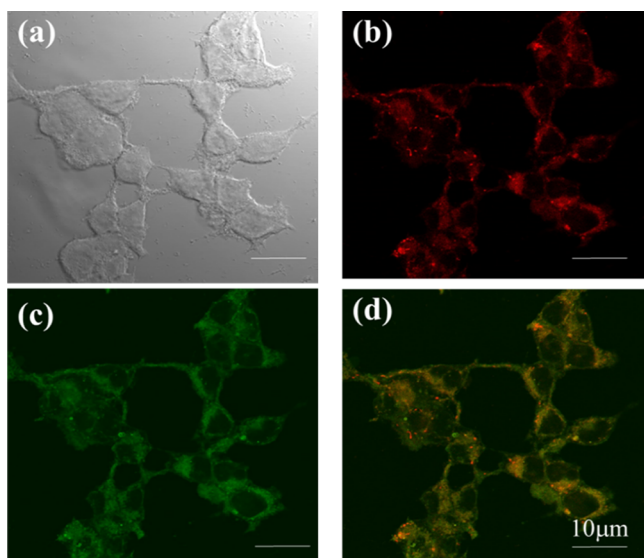
Figure 6. Bar diagram giving the IC<sub>50</sub> values of the complexes 1a–3a in dark and light in MCF-7 and HeLa cells (the light source is 400–700 nm Luzchem photoreactor of power 10 J cm<sup>-2</sup> and 1 h exposure time at 37 °C). Color codes: in dark, black; in light, green. Asterisk (\*) symbol indicates up to 100 μM complex concentration for which the corresponding complex does not reach IC<sub>50</sub>.

photo-cytotoxicity in both the cell lines but remained less toxic in the dark thus signifying their PDT effect. The IC<sub>50</sub> values of complex 1a in light of 400–700 nm were within 8.8–15.5 μM. The values for complex 2a in light were lower within 5.8–6.1 μM due to the presence of BODIPY as an additional photoactive moiety, while 1a had only curcumin as the photosensitizer. The photo-cytotoxicity of 3a was found to be excellent giving IC<sub>50</sub> values within 2.4–2.7 μM. This is due to higher ROS generation ability of the diiodo-BODIPY ligand. The IC<sub>50</sub> values of 3a are similar to those of the clinically approved PDT drug Photofrin.<sup>62,63</sup> The photo-cytotoxicity of the complexes follows the order of 3a ≫ 2a > 1a. The data

correspond to the ROS generation ability of the ligands: diiodoBODIPY-dpa ≫ BODIPY-dpa ≈ curcumin. The ligand dpa is photoinactive. A comparison of the IC<sub>50</sub> values of 1a and 2a suggest significant PDT activity of curcumin in metal-bound form. The objective of using a BODIPY unit in 2a is to utilize its emission property for cellular imaging, while the diiodo-BODIPY is incorporated to generate singlet oxygen, which is of paramount importance in PDT. The curcumin ligand, in contrast, generates primarily hydroxyl radicals on photo-activation. The aspect of singlet oxygen versus hydroxyl radical generation was probed from the mechanistic studies of the light-activated pUC19 DNA cleavage reactions (vide infra). The photoactivity of the BODIPY ligands L<sub>1</sub> and L<sub>2</sub> alone could not be studied with accuracy because of their poor aqueous solubility. Curcumin (Hcur) alone showed significant photocytotoxicity in cervical HeLa cells on short incubation time of 4 h in DMEM medium giving an overall order of 3a ≫ 2a > Hcur > 1a (Table 4). The dye alone showed significant degradation on longer incubation time in the buffer medium as evidenced from the spectral studies.

**Mitochondrial Localization.** Subcellular localization study in MCF-7 cells was performed by confocal microscopy using emissive complexes 1a ( $\phi_F = 0.04$ ) having photoactive curcumin (Figure S23, Supporting Information) and 2a having both photoactive BODIPY and curcumin moieties ( $\phi_F = 0.11$ ) (Figure 7). From the merged images it is evident that the complexes predominantly colocalized giving overlap coefficient value of ~0.7 with the Mito Tracker Deep Red (MTR) indicating their selective localization in the mitochondria of the cells. This observation is of importance, as both curcumin and BODIPY dyes are known to target mitochondria as is observed for the PDT drug Photofrin.<sup>7,31,62,66</sup> Anticancer agents localizing in the mitochondria can avoid the deactivation pathway associated with the nuclear DNA targeting drugs by nuclear excision repair (NER) mechanism.<sup>36,37</sup>

**Reactive Oxygen Species.** ROS plays very important role to induce apoptotic cell death. The complexes were found to induce cell cycle arrest of MCF-7 cells in G1-S phase, and apoptotic death of the cells by 3a was confirmed by annexin-V FITC and propidium iodide (PI) assays (Figures S24 and S25, Supporting Information). Generation of any ROS by the complexes 1a–3a on exposure to visible light (400–700 nm)



**Figure 7.** Confocal microscopic images of MCF-7 cells after 4 h of incubation with complex **2a**: (a) bright field, (b) fluorescence of MTR, (c) fluorescence of **2a**, and (d) merged image of (b, c). Scale bar = 10  $\mu\text{m}$ .

was probed in MCF-7 cells by DCFDA assay. DCFDA is a cell-permeable fluorogenic probe. It gets oxidized to DCF in presence of ROS and displays emission maxima at 528 nm.<sup>67</sup> Enhanced ROS generation leads to increase in the DCF-based emission intensity, which could be quantified from flow cytometry data. The assay data on MCF-7 cells showed significant increase in DCF based emission for the complex **3a** treated cells with light (400–700 nm) for 1 h of irradiation, while formation of DCF was insignificant in absence of light (Figure S26, Supporting Information). The ROS generated could be singlet oxygen via a type-II process or hydroxyl radicals via photoredox pathway.<sup>30–32</sup> DPBF experiment was performed to ascertain formation of any singlet oxygen. DPBF is known to react with singlet oxygen ( $^1\text{O}_2$ ) to form endoperoxide, and a decrease in the DPBF based absorption intensity at 417 nm indicates formation of  $^1\text{O}_2$ . Ligand  $\text{L}_2$  and complex **3** of this ligand showed similar and rapid decay of the DPBF absorbance on visible light (400–700 nm) irradiation with lower complex concentration (Figure 8, Figure S27, Supporting Information). The presence of two heavy iodine atoms in ligand  $\text{L}_2$  makes the ISC favorable thus stabilizing the

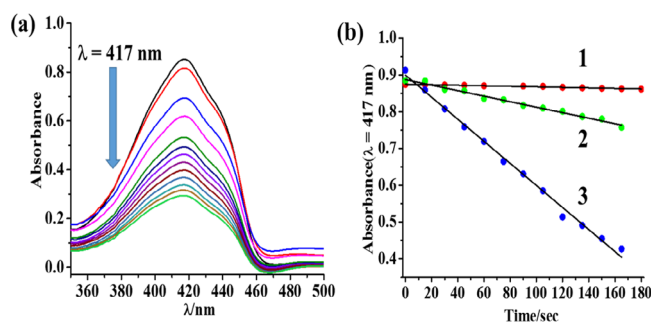


**Figure 8.** (a) Absorption spectral traces of DPBF and complex **3** (0.1  $\mu\text{M}$ ) on exposure to light (400–700 nm,  $10 \text{ J}\cdot\text{cm}^{-2}$ ) for exposure time of 15 s. (b) Plot showing changes in absorbance of DPBF at 417 nm with time on light exposure with complexes **1–3**. A higher slope indicates more quantity of singlet oxygen generation.

triplet state, which by type-II energy transfer pathway generates singlet oxygen.<sup>57,58</sup> The singlet oxygen quantum yield value ( $\phi_{\Delta}$ ) for the iodinated BODIPY ligand ( $\text{L}_2$ ) is reported as 0.8.<sup>68</sup> Complex **1** having only curcumin as the photoactive moiety did not show any significant singlet oxygen generation. The ROS involved for this complex could be hydroxyl radicals as reported for other curcumin–metal complexes.<sup>21,22</sup> The decay rate for complex **2** for DPBF absorbance ( $7.5 \times 10^{-4} \text{ s}^{-1}$ ) was found to be significantly lower and  $\sim 25\%$  of that of the complex **3** ( $3.0 \times 10^{-3} \text{ s}^{-1}$ ; Figure 8b).

**DNA Binding and Cleavage.** Confocal microscopic images showed that the complexes primarily located at the mitochondria of the cells. Targeting mitochondria has several positive aspects: (i) being the powerhouse of cell, mitochondrial damage arrests rapid growth of cancerous cells, (ii) NER mechanism is absent in mitochondrial circular DNA, (iii) many significant metabolisms of cancer cells get affected as they take place in this important organelle, and (iv) release of cytochrome-c from mitochondria to the cytoplasm leads to initiate caspase-dependent apoptotic cell death. Mitochondrial DNA being a potential target of the complexes, the interaction of **1a–3a** with ct-DNA was studied by UV–vis absorption and viscosity experiments. The intrinsic binding constants ( $K_b$ ) of the complexes for ct-DNA were  $\sim 1 \times 10^5 \text{ M}^{-1}$  in 5% DMF–Tris buffer (pH = 7.2) giving an order of **2a** > **1a** > **3a** (Figures S28–S30, Supporting Information). Free curcumin is known to show weak intercalative mode of binding with herring sperm DNA (hs-DNA), and dimethoxycurcumin (Dimc), a synthetic analogue of native curcumin, exhibits minor groove binding property with ct-DNA.<sup>69,70</sup> From the plot of  $(\eta/\eta_0)^{1/3}$  versus  $[\text{complex}]/[\text{DNA}]$  using viscometric titration data of the complexes in DMF–Tris–HCl buffer (pH = 7.2) and ct-DNA at 37  $^\circ\text{C}$  it appears that the complexes are partial intercalative ct-DNA binders considering ethidium bromide (EB) and Hoechst dye as standard DNA intercalator and groove binder, respectively (Figure S31, Supporting Information). DNA binding properties of the complexes studied by EB displacement and emission quenching method gave  $K_{\text{app}}$  values of  $(3.4 \pm 0.8) \times 10^4 \text{ M}^{-1}$ ,  $(4.4 \pm 0.8) \times 10^4 \text{ M}^{-1}$  and  $(3.2 \pm 0.2) \times 10^4 \text{ M}^{-1}$  for **1a–3a**, respectively, giving an order of **2a** > **1a**  $\approx$  **3a** (Figures S32–S34, Supporting Information).

Photoinduced DNA cleavage activity of the complexes (**1a–3a**) and the ligands (Hcur,  $\text{L}_1$  and  $\text{L}_2$ ) was studied (taking 10  $\mu\text{M}$  concentration of each sample) with dark controls using SC pUC19 DNA (30  $\mu\text{M}$ , 0.2  $\mu\text{g}$ ) in Tris–HCl/NaCl (50 mM, pH = 7.2) buffer (Figure 9A, Figure S34, Supporting Information). Gel electrophoresis in agarose gel was done to assess the extent of nicked circular (NC) DNA formation from the SC DNA in presence of the complexes and ligands. Monochromatic visible light source of 532 nm (100 mW power) was used from a CW diode laser. The wavelength chosen for the DNA photocleavage activity is based on the presence of the BODIPY-centered electronic spectral band of the complexes **2a** and **3a** near 501 and 535 nm, respectively. Each sample, after treating with the DNA solution in Tris–HCl buffer medium, was incubated for 1 h in the dark, followed by 1 h of exposure to light. The complexes and ligands (10  $\mu\text{M}$ ) did not show any significant DNA cleavage activity ( $\leq 10\%$  NC) in the dark. However, formation of 9, 20, and 50% of NC DNA was observed in presence of light for the ligands Hcur,  $\text{L}_1$ , and  $\text{L}_2$  alone, respectively. Complexes **1a–3a** gave, respectively, 42, 60, and 90% of NC DNA under similar experimental conditions.

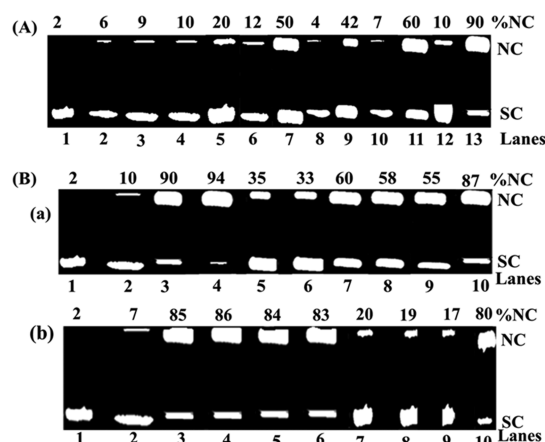


**Figure 9.** (A) Gel electrophoresis diagram showing the cleavage of pUC19 DNA (0.2  $\mu\text{g}$ , 30  $\mu\text{M}$  base pair) by the complexes **1a–3a**, ligands Hcur,  $L_1$ , and  $L_2$  (10  $\mu\text{M}$ ) in light of 532 nm (100 mW, 1 h exposure): lane 1, DNA control (L); lanes 2 and 3, Hcur (D) and HCur (L); lanes 4 and 5,  $L_1$  (D) and  $L_1$  (L); lanes 6 and 7,  $L_2$  (D) and  $L_2$  (L); lanes 8 and 9, **1a** (D) and **1a** (L); lanes 10 and 11, **2a** (D) and **2a** (L); lanes 12 and 13, **3a** (D) and **3a** (L), where L is for light-exposed and D is under dark condition. (B) Mechanistic data for cleavage of pUC19 DNA (0.2  $\mu\text{g}$ , 30  $\mu\text{M}$  base pair) by (a) **3a** (10  $\mu\text{M}$ ) and (b) **1a** (25  $\mu\text{M}$ ) in light of 532 nm (100 mW, 1 h exposure time): lane 1, pUC19 DNA control; lane 2, complex in dark; lane 3, complex in light; lanes 4–10 are for the complexes in the presence of various additives: lane 4,  $\text{D}_2\text{O}$  (16  $\mu\text{L}$ ); lane 5,  $\text{NaN}_3$  (0.5 mM); lane 6, TEMP (0.5 mM); lane 7, DMSO (4  $\mu\text{L}$ ); lane 8, KI (0.5 mM); lane 9, catalase (4  $\mu\text{L}$ ); and lane 10, SOD (4 units).

For the mechanistic study of ROS generation, complexes **3a** (10  $\mu\text{M}$ ) and **1a** (25  $\mu\text{M}$ ) were treated with pUC-19 DNA and photoexposed in presence of different singlet oxygen quenchers, hydroxyl radical scavengers, and SOD as superoxide radical scavenger (Figure 9B, Figures S35–S37, Supporting Information). Complex **3a** in  $\text{D}_2\text{O}$  showed higher percentage of NC DNA (94%), whereas in presence of singlet oxygen quenchers like  $\text{NaN}_3$  and TEMP it was diminished to 30%. In contrast, hydroxyl radical scavengers like KI, DMSO, and catalase showed minor reduction giving 60% of NC DNA. No significant decrease in percentage of NC DNA was observed in presence of SOD. Complex **1a** (25  $\mu\text{M}$ ), in contrast, showed no apparent change in the percentage of NC DNA in presence of  $\text{D}_2\text{O}$  or on addition of  $\text{NaN}_3$  or TEMP. However, a significant reduction in NC DNA from 85% to 20% was observed in presence of hydroxyl radical scavengers like KI, DMSO, and catalase. A minor reduction in %NC DNA was also observed in presence of SOD. The mechanistic study reveals that complex **3a** having both diiodo BODIPY and curcumin produces both singlet oxygen ( $\sim 70\%$ ) and hydroxyl radicals ( $\sim 30\%$ ) on photoactivation. Complex **1a** having only dpa produces primarily hydroxyl radicals as the ROS. That makes complex **3a** a novel vanadium-based PDT agent with curcumin retaining its pendant diphenolic moieties. DNA photocleavage studies reveal that the extent of total ROS generation for **1a** and **2a** are  $\sim 47\%$  and  $\sim 66\%$  than that of **3a** in similar experimental condition in presence of light, which is in good agreement with the DCFDA assay demonstrating that an enhancement in DCF-based emission intensity in light is distinctly greater in case of complex **3a** in comparison to the other two complexes (Figure S26, Supporting Information).

## CONCLUSIONS

This work presents a structurally characterized ternary oxidovanadium(IV) complex of curcumin and dipicolylamine (dpa) along with its analogues having pendant photoactive BODIPY moieties showing visible light-induced (400–700 nm, 10  $\text{J cm}^{-2}$ ) cytotoxicity in MCF-7 and HeLa cells. The observed photoactivity is akin to the PDT effect reported for the United States Food and Drug Administration-approved hematoporphyrin drug Photofrin. Interestingly, the complexes remained less toxic in the dark. The emissive complexes were used for cellular imaging. They showed primarily mitochondrial localization and cellular death via apoptotic pathway involving ROS. This observation is of importance, as nuclear targeting anticancer agents like cisplatin and analogues suffer from intrinsic resistance of cells. While the complex having dpa showed light-induced formation of hydroxyl radicals as the ROS via photoredox pathway, the diiodo BODIPY moiety displayed significant generation of singlet oxygen as the ROS via type-II process as evidenced from the mechanistic data obtained from the pUC19 DNA photocleavage studies. The complexes were stable in the physiological buffer medium without showing any apparent dissociation and degradation of the curcumin ligand. Binding of curcumin to the oxophilic  $\text{VO}^{2+}$  moiety has significantly enhanced its stability. The presence of curcumin and photoactive BODIPY moieties as the photosensitizers to the oxidovanadium(IV) moiety in the ternary structure has resulted to a significant enhancement in its photo-cytotoxic potential under physiological conditions. Curcumin retaining its therapeutic potential under in vitro cellular conditions is of importance for any in vivo applications, as the drug in itself is categorized under “PAINS” due to its hydrolytic instability and poor bioavailability. Further studies are on to understand any specific role the “drug” plays with its intact diphenolic moiety in the apoptotic cell death mechanism.

## ASSOCIATED CONTENT

### Supporting Information

The Supporting Information is available free of charge on the ACS Publications website at DOI: 10.1021/acs.inorgchem.7b01924.

Details of the experimental procedures, reaction scheme, ESI-MS, IR spectra, d–d transitions of **1–3**, cyclic voltammograms, UV–visible stability data, ESI-MS of complexes, crystal structure (ORTEP and unit-cell packing diagrams showing H-bonding), electronic transitions by DFT, time-dependent cellular incorporation assay, MTT assay plots, confocal images of **1a**, cell cycle profiles of **1a–3a**, Annexin assay profile of **3a**, DCFDA assay, DPBF absorbance decay plots, DNA binding data, DNA photocleavage bar diagrams, DFT data for the complexes, a list of M–O(Cur) bond distances of structurally characterized curcumin complexes (PDF)

### Accession Codes

CCDC 1543636 contains the supplementary crystallographic data for this paper. These data can be obtained free of charge via [www.ccdc.cam.ac.uk/data\\_request/cif](http://www.ccdc.cam.ac.uk/data_request/cif), or by emailing [data\\_request@ccdc.cam.ac.uk](mailto:data_request@ccdc.cam.ac.uk), or by contacting The Cambridge Crystallographic Data Centre, 12 Union Road, Cambridge CB2 1EZ, UK; fax: +44 1223 336033.

## ■ AUTHOR INFORMATION

## Corresponding Authors

\*E-mail: [paturu@mrdg.iisc.ernet.in](mailto:paturu@mrdg.iisc.ernet.in). Phone: +91-80-22932688. Fax: +91-80-23600999. (P.K.)

\*E-mail: [arc@ipc.iisc.ernet.in](mailto:arc@ipc.iisc.ernet.in). Phone: +91-80-22932533. Fax: +91-80-23600683. (A.R.C.)

ORCID 

Samya Banerjee: 0000-0003-4393-4447

Akhil R. Chakravarty: 0000-0002-6471-9167

## Notes

The authors declare no competing financial interest.

## ■ ACKNOWLEDGMENTS

The authors thank the Department of Science and Technology (DST), Government of India, for financial support (Grant Nos. SR/SS/MBD-02/2007 and EMR/2015/000742). The authors also thank the Alexander von Humboldt (AvH) Foundation, Germany, for an electrochemical system. A.R.C. thanks the DST for a J. C. Bose national fellowship. P.K.'s research group is funded by DBT-IISc grants. We thank Dr. Uttara, Urvasi, and Deepika for FACS data and Saima and Santosh for confocal microscopy images.

## ■ REFERENCES

- (1) Aggarwal, B. B.; Sung, B. Pharmacological Basis for the Role of Curcumin in Chronic Diseases: An Age-Old Spice with Modern Targets. *Trends Pharmacol. Sci.* **2009**, *30*, 85–94.
- (2) Aggarwal, B. B.; Harikumar, K. B. Potential Therapeutic Effects of Curcumin, the Anti-inflammatory Agent, Against Neurodegenerative, Cardiovascular, Pulmonary, Metabolic, Autoimmune and Neoplastic Diseases. *Int. J. Biochem. Cell Biol.* **2009**, *41*, 40–59.
- (3) Craggs, L.; Kalara, R. N. Revisiting Dietary Antioxidants, Neurodegeneration and Dementia. *NeuroReport* **2011**, *22*, 1–3.
- (4) Chuengsamarn, S.; Rattanamongkolgul, S.; Luechapudiporn, R.; Phisalaphong, C.; Jirawatnotai, S. Curcumin Extract for Prevention of Type 2 Diabetes. *Diabetes Care* **2012**, *35*, 2121–2127.
- (5) Wilken, R.; Veena, M. S.; Wang, M. B.; Srivatsan, E. S. Curcumin: A Review of Anti-Cancer Properties and Therapeutic Activity in Head and Neck Squamous Cell Carcinoma. *Mol. Cancer* **2011**, *10*, 12–19.
- (6) Perrone, D.; Ardito, F.; Giannatempo, G.; Dioguardi, M.; Troiano, G.; Lo Russo, L.; De Lillo, A.; Laino, L.; Lo Muzio, L. Biological and Therapeutic Activities, and Anticancer Properties of Curcumin. *Exp. Ther. Med.* **2015**, *10*, 1615–1623.
- (7) Priyadarshini, K. I. The Chemistry of Curcumin: From Extraction to Therapeutic Agent. *Molecules* **2014**, *19*, 20091–20112.
- (8) Lal, J.; Gupta, S. K.; Thavaselvam, D.; Agarwal, D. D. Design, Synthesis, Synergistic Antimicrobial Activity and Cytotoxicity of 4-aryl substituted 3,4-dihydropyrimidinones of Curcumin. *Bioorg. Med. Chem. Lett.* **2012**, *22*, 2872–2876.
- (9) Shehzad, A.; Wahid, F.; Lee, Y. S. Curcumin in Cancer Chemoprevention: Molecular Targets, Pharmacokinetics, Bioavailability, and Clinical Trials. *Arch. Pharm. (Weinheim, Ger.)* **2010**, *343*, 489–499.
- (10) Hatcher, H.; Planalp, R.; Cho, J.; Torti, F. M.; Torti, S. V. Curcumin: From Ancient Medicine to Current Clinical Trials. *Cell. Mol. Life Sci.* **2008**, *65*, 1631–1652.
- (11) Shishodia, S.; Amin, H. M.; Lai, R.; Aggarwal, B. B. Curcumin (Diferuloylmethane) Inhibits Constitutive NF- $\kappa$ B Activation, Induces G1/S Arrest, Suppresses Proliferation, and Induces Apoptosis in Mantle Cell Lymphoma. *Biochem. Pharmacol.* **2005**, *70*, 700–713.
- (12) Mishra, A.; Kumar, R.; Tyagi, A.; Kohaar, I.; Hedau, S.; Bharti, A. C.; Sarker, S.; Dey, D.; Saluja, D.; Das, B. Curcumin Modulates Cellular AP-1, NF- $\kappa$ B, and HPV16 E6 Proteins in Oral Cancer. *Encancermedalscience* **2015**, *9*, 525–536.
- (13) Deng, Y.; Verron, E.; Rohanizadeh, R. Molecular Mechanisms of Anti-metastatic Activity of Curcumin. *Anticancer Res.* **2016**, *36*, 5639–5647.
- (14) Pavan, A. R.; Silva, G. D. B.; Jornada, D. H.; Chiba, D. E.; Fernandes, G. F. S.; Man Chin, C.; dos Santos, J. Unraveling the Anticancer Effect of Curcumin and Resveratrol. *Nutrients* **2016**, *8*, 628–677.
- (15) Yoysungnoen, P.; Wirachwong, P.; Changtam, C.; Suksamram, A.; Patumraj, S. Anti-Cancer and Anti-Angiogenic Effects of Curcumin and Tetrahydrocurcumin on Implanted Hepatocellular Carcinoma in Nude Mice. *World J. Gastroenterol.* **2008**, *14*, 2003–2009.
- (16) Guo, L.; Chen, X.; Hu, Y.; Yu, Z.; Wang, D.; Liu, J. Curcumin Inhibits Proliferation and Induces Apoptosis of Human Colorectal Cancer Cells by Activating the Mitochondria Apoptotic Pathway. *Phytother. Res.* **2013**, *27*, 422–430.
- (17) Esatbeyoglu, T.; Huebbe, P.; Ernst, I. M. A.; Chin, D.; Wagner, A. E.; Rimbach, G. Curcumin-from Molecule to Biological Function. *Angew. Chem., Int. Ed.* **2012**, *51*, 5308–5332.
- (18) Nelson, K. M.; Dahlin, J. L.; Bisson, J.; Graham, J.; Pauli, G. F.; Walters, M. A. The Essential Medicinal Chemistry of Curcumin. *J. Med. Chem.* **2017**, *60*, 1620–1637.
- (19) Baell, J. B. Feeling Nature's PAINS: Natural Products, Natural Product Drugs, and Pan Assay Interference Compounds (PAINS). *J. Nat. Prod.* **2016**, *79*, 616–628.
- (20) Padmanaban, G.; Nagaraj, V. A. Curcumin May Defy Medicinal Chemists. *ACS Med. Chem. Lett.* **2017**, *8*, 274–274.
- (21) Banerjee, S.; Dixit, A.; Karande, A. A.; Chakravarty, A. R. Remarkable Selectivity and Photo-Cytotoxicity of an Oxidovanadium(IV) Complex of Curcumin in Visible Light. *Eur. J. Inorg. Chem.* **2015**, 447–457.
- (22) Banerjee, S.; Pant, I.; Khan, I.; Prasad, P.; Hussain, A.; Kondaiah, P.; Chakravarty, A. R. Remarkable Enhancement in Photocytotoxicity and Hydrolytic Stability of Curcumin on Binding to an Oxovanadium(IV) Moiety. *Dalton Trans.* **2015**, *44*, 4108–4122.
- (23) Garai, A.; Pant, I.; Banerjee, S.; Banik, B.; Kondaiah, P.; Chakravarty, A. R. Photorelease and Cellular Delivery of Mitocurcumin from Its Cytotoxic Cobalt(III) Complex in Visible Light. *Inorg. Chem.* **2016**, *55*, 6027–6035.
- (24) Renfrew, A. K.; Bryce, N. S.; Hambley, T. Cobalt(III) Chaperone Complexes of Curcumin: Photoreduction, Cellular Accumulation and Light-Selective Toxicity towards Tumour Cells. *Chem. - Eur. J.* **2015**, *21*, 15224–15234.
- (25) Pucci, D.; Crispini, A.; Sanz Mendiguchía, B.; Pirillo, S.; Ghedini, M.; Morelli, S.; De Bartolo, L. Improving the Bioactivity of Zn(II)-Curcumin Based Complexes. *Dalton Trans.* **2013**, *42*, 9679–9687.
- (26) Pettinari, R.; Marchetti, F.; Condello, F.; Pettinari, C.; Lupidi, G.; Scopelliti, R.; Mukhopadhyay, S.; Riedel, T.; Dyson, P. J. Ruthenium(II)-Arene RAPTA Type Complexes Containing Curcumin and Bisdemethoxycurcumin Display Potent and Selective Anticancer Activity. *Organometallics* **2014**, *33*, 3709–3715.
- (27) Mitra, K.; Gautam, S.; Kondaiah, P.; Chakravarty, A. R. The Cis-Diammineplatinum(II) Complex of Curcumin: A Dual Action DNA Crosslinking and Photochemotherapeutic Agent. *Angew. Chem., Int. Ed.* **2015**, *54*, 13989–13993.
- (28) Raza, M. K.; Mitra, K.; Shettar, A.; Basu, U.; Kondaiah, P.; Chakravarty, A. R. Photoactive Platinum(II)  $\beta$ -diketonates as Dual Action Anticancer Agents. *Dalton Trans.* **2016**, *45*, 13234–13243.
- (29) Hussain, A.; Somyajit, K.; Banik, B.; Banerjee, S.; Nagaraju, G.; Chakravarty, A. R. Enhancing the Photocytotoxic Potential of Curcumin on Terpyridyl Lanthanide(III) Complex Formation. *Dalton Trans.* **2013**, *42*, 182–195.
- (30) Banerjee, S.; Chakravarty, A. R. Metal Complexes of Curcumin for Cellular Imaging, Targeting, and Photoinduced Anticancer Activity. *Acc. Chem. Res.* **2015**, *48*, 2075–2083.
- (31) Dolmans, D. E. J. G. J.; Fukumura, D.; Jain, R. K. Photodynamic therapy for cancer. *Nat. Rev. Cancer* **2003**, *3*, 381–387.

- (32) Issa, M.; Manela-Azulay, M. Photodynamic Therapy: A Review of the Literature and Image Documentation. *An. Bras. Dermatol.* **2010**, *85*, 501–511.
- (33) Szacilowski, K.; Macyk, W.; Drzewiecka-Matuszek, A.; Brindell, M.; Stochel, G. Bioinorganic Photochemistry: Frontiers and Mechanisms. *Chem. Rev.* **2005**, *105*, 2647–2694.
- (34) Kamkaew, A.; Lim, S. H.; Lee, H. B.; Kiew, L. V.; Chung, L. Y.; Burgess, K. BODIPY Dyes in Photodynamic Therapy. *Chem. Soc. Rev.* **2013**, *42*, 77–88.
- (35) Mehraban, N.; Freeman, H. S. Developments in PDT Sensitizers for Increased Selectivity and Singlet Oxygen Production. *Materials* **2015**, *8*, 4421–4456.
- (36) Cline, S. D. Mitochondrial DNA Damage and its Consequences for Mitochondrial Gene Expression. *Biochim. Biophys. Acta, Gene Regul. Mech.* **2012**, *1819*, 979–991.
- (37) Kazak, L.; Reyes, A.; Holt, I. J. Minimizing the Damage: Repair Pathways Keep Mitochondrial DNA Intact. *Nat. Rev. Mol. Cell Biol.* **2012**, *13*, 659–671.
- (38) Perrin, D. D.; Armarego, W. L. F.; Perrin, D. R. *Purification of Laboratory Chemicals*; Pergamon Press: Oxford, UK, 1980.
- (39) Kottol, K.; Varghese, N.; Pushpakumari, K. N. Purification and Separation of Individual Curcuminoids from Spent Turmeric Oleoresin, a by-Product from Curcumin Production Industry. *International J. Pharm. Sci. Res.* **2014**, *5*, 3246–3254.
- (40) Michel, B. W.; Lippert, A. R.; Chang, C. J. A Reaction-Based Fluorescent Probe for Selective Imaging of Carbon Monoxide in Living Cells Using a Palladium-Mediated Carbonylation. *J. Am. Chem. Soc.* **2012**, *134*, 15668–15671.
- (41) Bhattacharyya, A.; Dixit, A.; Mitra, K.; Banerjee, S.; Karande, A. A.; Chakravarty, A. R. BODIPY Appended Copper(II) Complexes of Remarkable Photocytotoxicity in Visible Light. *MedChemComm* **2015**, *6*, 846–851.
- (42) Williams, A. T. R.; Winfield, S. A.; Miller, J. N. Relative Fluorescence Quantum Yields Using a Computer-Controlled Luminescence Spectrometer. *Analyst* **1983**, *108*, 1067–1071.
- (43) Miller, G. J.; Lin, J.; Young, V., Jr. Structure and Bonding in  $[\text{TaCl}_4(\text{C}_5\text{H}_5\text{N})_2]$ . *Acta Crystallogr., Sect. C: Cryst. Struct. Commun.* **1993**, *49*, 1770–1773.
- (44) Sheldrick, G. M. *SHELX-2014*, Programs for Crystal Structure Solution and Refinement; University of Göttingen: Göttingen, Germany, 2014.
- (45) Farrugia, L. J. WinGX Suite for Small-Molecule Single-Crystal Crystallography. *J. Appl. Crystallogr.* **1999**, *32*, 837–838.
- (46) Becke, A. D. Density-Functional Exchange-Energy Approximation with Correct Asymptotic Behavior. *Phys. Rev. A: At., Mol., Opt. Phys.* **1988**, *38*, 3098–3100.
- (47) Wadt, W. R.; Hay, P. J. Ab Initio Effective Core Potentials for Molecular Calculations. Potentials for Main Group Elements Na to Bi. *J. Chem. Phys.* **1985**, *82*, 284–298.
- (48) Frisch, M. J.; Trucks, G. W.; Schlegel, H. B.; Scuseria, G. E.; Robb, M. A.; Cheeseman, J. R.; Montgomery, J. A., Jr.; Vreven, T.; Kudin, K. N.; Burant, J. C.; Millam, J. M.; Iyengar, S. S.; Tomasi, J.; Barone, V.; Mennucci, B.; Cossi, M.; Scalmani, G.; Rega, N.; Petersson, G. A.; Nakatsuji, H.; Hada, M.; Ehara, M.; Toyota, K.; Fukuda, R.; Hasegawa, J.; Ishida, M.; Nakajima, T.; Honda, Y.; Kitao, O.; Nakai, H.; Klene, M.; Li, X.; Knox, J. E.; Hratchian, H. P.; Cross, J. B.; Bakken, V.; Adamo, C.; Jaramillo, J.; Gomperts, R.; Stratmann, R. E.; Yazyev, O.; Austin, A. J.; Cammi, R.; Pomelli, C.; Ochterski, J. W.; Ayala, P. Y.; Morokuma, K.; Voth, G. A.; Salvador, P.; Dannenberg, J. J.; Zakrzewski, V. G.; Dapprich, S.; Daniels, A. D.; Strain, M. C.; Farkas, O.; Malick, D. K.; Rabuck, A. D.; Raghavachari, K.; Foresman, J. B.; Ortiz, J. V.; Cui, Q.; Baboul, A. G.; Clifford, S.; Cioslowski, J.; Stefanov, B. B.; Liu, G.; Liashenko, A.; Piskorz, P.; Komaromi, I.; Martin, R. L.; Fox, D. J.; Keith, T.; Al-Laham, M. A.; Peng, C. Y.; Nanayakkara, A.; Challacombe, M.; Gill, P. M. W.; Johnson, B.; Chen, W.; Wong, M. W.; Gonzalez, C.; Pople, J. A. *Gaussian 03*, revision B.4; Gaussian Inc.: Pittsburgh, PA, 2003.
- (49) Kumar, A.; Dixit, A.; Banerjee, S.; Bhattacharyya, A.; Garai, A.; Karande, A. A.; Chakravarty, A. R. Cellular Imaging and Mitochondria Targeted Photo-Cytotoxicity in Visible Light by Singlet Oxygen Using a BODIPY-Appended Oxovanadium(IV) DNA Crosslinking Agent. *MedChemComm* **2016**, *7*, 1398–1404.
- (50) Lau, J. T. F.; Lo, P. C.; Jiang, X. J.; Wang, Q.; Ng, D. K. P. A Dual Activatable Photosensitizer toward Targeted Photodynamic Therapy. *J. Med. Chem.* **2014**, *57*, 4088–4097.
- (51) Basu, U.; Pant, I.; Hussain, A.; Kondaiah, P.; Chakravarty, A. R. Iron(III) Complexes of a Pyridoxal Schiff Base for Enhanced Cellular Uptake with Selectivity and Remarkable Photocytotoxicity. *Inorg. Chem.* **2015**, *54*, 3748–3758.
- (52) Roy, S.; Patra, A. K.; Dhar, S.; Chakravarty, A. R. Photosensitizer in a Molecular Bowl and Its Effect on the DNA-Binding and -Cleavage Activity of 3d-Metal Scorpionates. *Inorg. Chem.* **2008**, *47*, S625–S633.
- (53) Merkel, P. B.; Nilsson, R.; Kearns, D. R. Deuterium Effects on Singlet Oxygen Lifetimes in Solutions. New Test of Singlet Oxygen Reactions. *J. Am. Chem. Soc.* **1972**, *94*, 1030–1031.
- (54) Geary, W. J. The Use of Conductivity Measurements in Organic Solvents. *Coord. Chem. Rev.* **1971**, *7*, 81–122.
- (55) Nakamoto, K. *Infrared and Raman Spectra of Inorganic and Coordination Compounds*; John Wiley and Sons: New York, 1997.
- (56) Banerjee, S.; Prasad, P.; Hussain, A.; Khan, I.; Kondaiah, P.; Chakravarty, A. R. Remarkable Photocytotoxicity of Curcumin in HeLa Cells in Visible Light and Arresting its Degradation on Oxovanadium(IV) Complex Formation. *Chem. Commun.* **2012**, *48*, 7702–7704.
- (57) Li, X.; Kolemen, S.; Yoon, J.; Akkaya, E. U. Activatable Photosensitizers: Agents for Selective Photodynamic Therapy. *Adv. Funct. Mater.* **2017**, *27*, 1604053–1604063.
- (58) Sabatini, R. P.; McCormick, T. M.; Lazarides, T.; Wilson, K. C.; Eisenberg, R.; McCamant, D. W. Intersystem Crossing in Halogenated Bodipy Chromophores Used for Solar Hydrogen Production. *J. Phys. Chem. Lett.* **2011**, *2*, 223–227.
- (59) Yogo, T.; Urano, Y.; Ishitsuka, Y.; Maniwa, F.; Nagano, T. Highly Efficient and Photostable Photosensitizer Based on BODIPY Chromophore. *J. Am. Chem. Soc.* **2005**, *127*, 12162–12163.
- (60) Banfi, S.; Nasini, G.; Zaza, S.; Caruso, E. Synthesis and Photo-Physical Properties of a Series of BODIPY Dyes. *Tetrahedron* **2013**, *69*, 4845–4856.
- (61) Gibbs, J. H.; Zhou, Z.; Kessel, D.; Fronczek, F. R.; Pakhomova, S.; Vicente, M. G. H. Synthesis, Spectroscopic, and in Vitro Investigations of 2,6-Diiodo-BODIPYs with PDT and Bioimaging Applications. *J. Photochem. Photobiol., B* **2015**, *145*, 35–47.
- (62) Ménard, F.; Sol, V.; Ringot, C.; Granet, R.; Alves, S.; Morvan, C.; Le Queneau, Y.; Ono, N.; Krausz, P. Synthesis of Tetraglucosyl- and Tetrapolyamine-Tetrazabenzoporphyrin Conjugates for an Application in PDT. *Bioorg. Med. Chem.* **2009**, *17*, 7647–7657.
- (63) Delaey, E.; Van Laar, F.; De Vos, D.; Kamuhabwa, A.; Jacobs, P.; De Witte, P. A Comparative Study of the Photosensitizing Characteristics of Some Cyanine Dyes. *J. Photochem. Photobiol., B* **2000**, *55*, 27–36.
- (64) Ott, I.; Schmidt, K.; Kircher, B.; Schumacher, P.; Wiglenda, T.; Gust, R. Antitumor-Active Cobalt-Alkyne Complexes Derived from Acetylsalicylic Acid: Studies on the Mode of Drug Action. *J. Med. Chem.* **2005**, *48*, 622–629.
- (65) Saha, S.; Majumdar, R.; Roy, M.; Dighe, R. R.; Chakravarty, A. R. An Iron Complex of Dipyrrophenazine as a Potent Photocytotoxic Agent in Visible Light. *Inorg. Chem.* **2009**, *48*, 2652–2663.
- (66) Kowada, T.; Maeda, H.; Kikuchi, K. BODIPY-Based Probes for the Fluorescence Imaging of Biomolecules in Living Cells. *Chem. Soc. Rev.* **2015**, *44*, 4953–4972.
- (67) Roesslein, M.; Hirsch, C.; Kaiser, J. P.; Krug, H. F.; Wick, P. Comparability of in Vitro Tests for Bioactive Nanoparticles: A Common Assay to Detect Reactive Oxygen Species as an Example. *Int. J. Mol. Sci.* **2013**, *14*, 24320–24337.
- (68) Bhattacharyya, A.; Dixit, A.; Banerjee, S.; Roy, B.; Kumar, A.; Karande, A.; Chakravarty, A. R. BODIPY Appended copper(II) Complexes for Cellular Imaging and Singlet Oxygen Mediated Anticancer Activity in Visible Light. *RSC Adv.* **2016**, *6*, 104474–104482.

(69) Li, X. L.; Hu, Y. J.; Mi, R.; Li, X. Y.; Li, P. Q.; Ouyang, Y. Spectroscopic Exploring the Affinities, Characteristics, and Mode of Binding Interaction of Curcumin with DNA. *Mol. Biol. Rep.* **2013**, *40*, 4405–4413.

(70) Kunwar, A.; Simon, E.; Singh, U.; Chittela, R. K.; Sharma, D.; Sandur, S. K.; Priyadarsini, I. K. Interaction of a Curcumin Analogue Dimethoxycurcumin with DNA. *Chem. Biol. Drug Des.* **2011**, *77*, 281–287.